Enhancing the High-Voltage Cycling Performance of LiNi$_{0.5}$Mn$_{0.3}$Co$_{0.2}$O$_2$ by Retarding Its Interfacial Reaction with an Electrolyte by Atomic-Layer-Deposited Al$_2$O$_3$

Yantao Su,[†] Suihan Cui,[†] Zengqing Zhuo,[†,‡] Wanli Yang,[‡] Xinwei Wang,*[,†] and Feng Pan*[,†]

[†]School of Advanced Materials, Peking University, Peking University Shenzhen Graduate School, Shenzhen 518055, China
[‡]Advanced Light Source (ALS), Lawrence Berkeley National Laboratory (LBNL), Berkeley, California 94720, United States

Ⓢ Supporting Information

ABSTRACT: High-voltage (>4.3 V) operation of Li-Ni$_x$Mn$_y$Co$_z$O$_2$ (NMC; $0 \leq x, y, z < 1$) for high capacity has become a new challenge for next-generation lithium-ion batteries because of the rapid capacity degradation over cycling. In this work, we investigate the performance of LiNi$_{0.5}$Mn$_{0.3}$Co$_{0.2}$O$_2$ (NMC532) electrodes with and without an atomic-layer-deposited (ALD) Al$_2$O$_3$ layer for charging/discharging in the range from 3.0 to 4.5 V (high voltage). The results of the electrochemical measurements show that the cells with ALD Al$_2$O$_3$-coated NMC532 electrodes have much enhanced cycling stability. The mechanism was investigated by using X-ray photoelectron spectroscopy, X-ray absorption spectroscopy, and electrochemical methods. We find that the ultrathin ALD Al$_2$O$_3$ film can reduce the interface resistance of lithium-ion diffusion and enhance the surface stability of NMC532 by retarding the reactions at NMC532/electrolyte interfaces for preventing the formation of a new microstructure rock-salt phase NiO around the NMC532 surfaces.

KEYWORDS: interfacial reaction, cycling performance, atomic layer deposition, lithium-ion battery, cathode materials
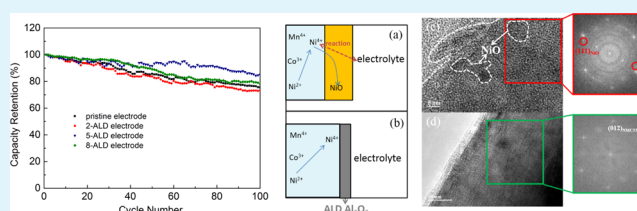
1. INTRODUCTION

Rechargeable lithium-ion batteries (LIBs) have drawn extensive attention because of their excellent properties, such as high energy density and lightweight. LiNi$_x$Mn$_y$Co$_z$O$_2$ (NMC; $0 \leq x, y, z < 1$) as the cathode material pioneered by Ohzuku and Makimura[1] and Dahn et al.[2] is comprised of alternating lithium and transition-metal layers, where the valence states of Ni, Mn, and Co are 2+, 4+, and 3+, respectively. NMC materials have shown high capacity, low cost, enhanced cycling stability, and improved safety performance; they have been regarded as suitable cathode materials for LIBs in low-emission hybrid electric vehicles (HEVs) and plug-in hybrid electric vehicles (PHEVs).[3]

Recently, in order to enhance the energy density of the NMC-cathode-based LIBs, researchers have suggested to raise the charge cutoff potential to higher voltage, such as 4.5 V, to further increase lithium extraction from NMC.[4−7] The challenge for cycling the NMC cathodes at higher voltages would result in significant deterioration of the LIBs. For example, a small amount of moisture contained in a commercial electrolyte can react with LiPF$_6$ to produce detrimental contaminants, such as HF, which can degrade the electrochemical performance because of the NMC/electrolyte interfacial reactions during charging/discharging cycling.[8−11] Typically, higher charge cutoff potential can accelerate the surface reconstruction of the cathode materials because of the interfacial reaction between the electrolyte and highly delithiated NMCs, leading to drastic interfacial dissolution of

the NMCs.[6,7,12,13] As a result, the use of high charge cutoff potentials on NMCs generally results in significant deterioration of the cycling performance and rate capability,[7,14−17] which hinders its potential applications in HEV and PHEV batteries. Thus, the surface structure of cathode materials and the interfacial interaction between the cathode and liquid electrolyte play two crucial roles in the electrochemical reactions and the performance of LIBs.[14]

Surface coating of NMCs is often used to improve the cycling performance by preventing electrolyte/electrode interfacial reactions and reducing the surface dissolution of NMC into the electrolyte.[18−23] As an effective surface coating method, atomic layer deposition (ALD) is a method of growing conformal thin films using sequential, self-limiting surface reactions. As demonstrated in previous works,[24] ALD offers an excellent advantage of precisely controlling the coating thickness by digitally adjusting the deposition cycles. ALD has many unique advantages for coating the surface of cathode and anode materials for LIBs. Very recently, efforts have been made on the ALD of metal oxides on cathodes,[8,18,20−23,25] anodes,[26,27] and separators[28] to increase their electrochemical performances. In the case of cathodes, several literatures have demonstrated that the electrochemical performance of LiCoO$_2$ cathodes can be improved by ALD.[8,20,21] NMC has become
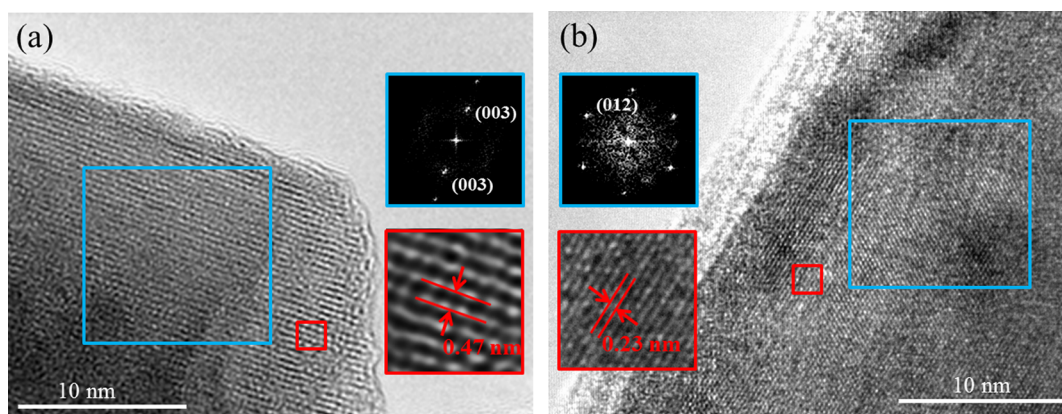
Figure 1. TEM images of (a) pristine and (b) 10-ALD electrodes. Insets: FFTs and lattice fringes.

one of the most important cathode materials for next-generation LIBs because of its high capacity and cost effectiveness compared to $LiCoO_2$. However, studies of ALD Al_2O_3 on the NMC materials are not only scarce[18] but also necessary from the aspect of cathode/electrolyte interfacial reactions.

In this study, we conduct an investigation on the effect of the ALD Al_2O_3 coating on commercial NMC532 cathode materials at higher voltage (about 4.5 V). Our results demonstrate that the controllable coating is very effective in improving the cycling stability of the NMC532 cathodes. When X-ray photoelectron spectroscopy (XPS), soft X-ray absorption spectroscopy (XAS), and electrochemical methods are combined, the mechanism of improvement is proposed to result from the ultrathin ALD Al_2O_3 film to retard the microstructural phase transitions and/or the electrode/electrolyte interfacial reactions.

2. EXPERIMENTAL SECTION

The pristine NMC532 electrodes were prepared by slurry coating on aluminum foils, which served as the current collectors. The slurry contained 80 wt % cathode materials (NMC532), 10 wt % carbon black, and 10 wt % poly(vinylidene difluoride) binder in *N*-methylpyrrolidinone solvent. To remove excess water, the slurry electrodes were dried in air at 80 °C for 1 h and then in a vacuum oven overnight at 110 °C.

ALD Al_2O_3 films were grown on the pristine NMC532 electrodes using a homemade ALD system at a deposition temperature of 120 °C. The precursors used for ALD Al_2O_3 were water and trimethylaluminum [TMA, $Al(CH_3)_3$].

The pristine NMC532 electrodes were placed in the reaction chamber. The ALD Al_2O_3 reaction cycle consisted of the following steps: (1) prepumping the chamber for 5 s, (2) delivering sufficient TMA for 1 s to allow the pressure to increase to 5 mbar, (3) purging the chamber with pure nitrogen for 120 s to completely remove the reaction byproducts and unreacted excess TMA, (4) delivering H_2O for 1 s to allow the pressure to increase to 5 mbar, and (5) purging the chamber with pure nitrogen for 120 s to completely remove the reaction byproducts and unreacted excess H_2O. The total ALD cycle number was varied from 2, 5, 8, to 10 cycles in order to deposit Al_2O_3 with different thicknesses on the cathodes (abbreviated as 2-ALD, 5-ALD, 8-ALD, and 10-ALD electrodes).

The morphology and microstructures of the ALD Al_2O_3 thin-film coatings were observed by field-emission scanning electron microscopy (Nova NanoSEM 450) and high-resolution transmission electron microscopy (HRTEM; FEI Tecnai G2 F20 S-Twin). XPS measurements were carried out on Thermo Fisher Scientific ESCALAB 250Xi system with monochromated Al Kα radiation to examine the changes of the surface compositions of the NMC532 electrodes with and

without the ALD coatings before and after charging and discharging to a high voltage of 4.5 V. During XPS data acquisition, a constant analyzer energy mode was used at a step size of 0.1 eV. To determine the changes of the compositions on the charged electrode surface, the coin cell was disassembled in an argon-filled glovebox, then washed several times with dimethyl carbonate, and then dried overnight in a vacuum oven. The C 1s peak (284.8 eV) from adventitious carbon was employed as the reference for binding energy calibration. Soft XAS was performed at beamline 8.0.1 of the ALS at LBNL. The undulator and spherical grating monochromator supplied a linearly polarized photon beam with resolving power up to 6000. The experimental energy resolution was better than 0.15 eV. All of the XAS experiments were performed at room temperature. All of the spectra were collected in both surface-sensitive total electron yield (TEY) and bulk-sensitive total fluorescence yield (TFY) modes. The probing depth for TEY was around 10 nm, and that of TFY was around 150 nm. All of the spectra were normalized to the photon flux measured by the photocurrent of an upstream gold mesh.

For electrochemical measurements, CR-2032-type coin cells were assembled in a glovebox under a dry argon atmosphere (moisture and oxygen levels of less than 1 ppm), in which the NMC532 electrodes, lithium foils, and Celgard-2502 membrane were used as the working (cathode) electrodes, the counter (anode) electrodes, and separators, respectively. The electrolyte was composed of 1 M $LiPF_6$ salt dissolved in ethylene carbonate/diethyl carbonate/ethylmethyl carbonate of 1:1:1 volume ratio. All assembled cells were allowed to rest for about 6 h for equilibrium prior to the electrochemical tests at room temperature. The cells were cycled at a constant current between 3.0 and 4.5 V versus Li/Li^+ (1 C equal to 170 mAh g^{-1}) using a Neware battery test system. Cyclic voltammetry (CV) measurements were performed on a CHI760D electrochemical potentiostat. Galvanostatic intermittent titration technique (GITT) measurements were carried out by a MACCOR battery test cabinet (model MC-16 battery test system; 5 V and 5 A). Electrochemical impedance spectroscopy (EIS) measurements were carried out on a Princeton Applied Research 2731 impedance analyzer with an amplitude voltage of 5 mV and a frequency range of 10 mHz to 100 kHz. In order to eliminate the influence of the formed thick solid electrolyte interface (SEI) from a lithium metal anode, especially at the high-frequency regime, we used a three-electrode cell (MTI Corp.) for impedance measurement. Before EIS measurements, all cells were initially charged to 4.5 V at 0.1 C rates. All of the electrochemical measurements were conducted at room temperature.

3. RESULTS AND DISCUSSION

In this study, the sizes of the particles of the commercial cathode NMC532 for ALD Al_2O_3 were in the range of 8−10 μm, consisting of many primary particles with sizes of 600 nm to 2 μm. ALD Al_2O_3-derived coating layers on the cathode electrodes were generated with uniform and dense coating, as
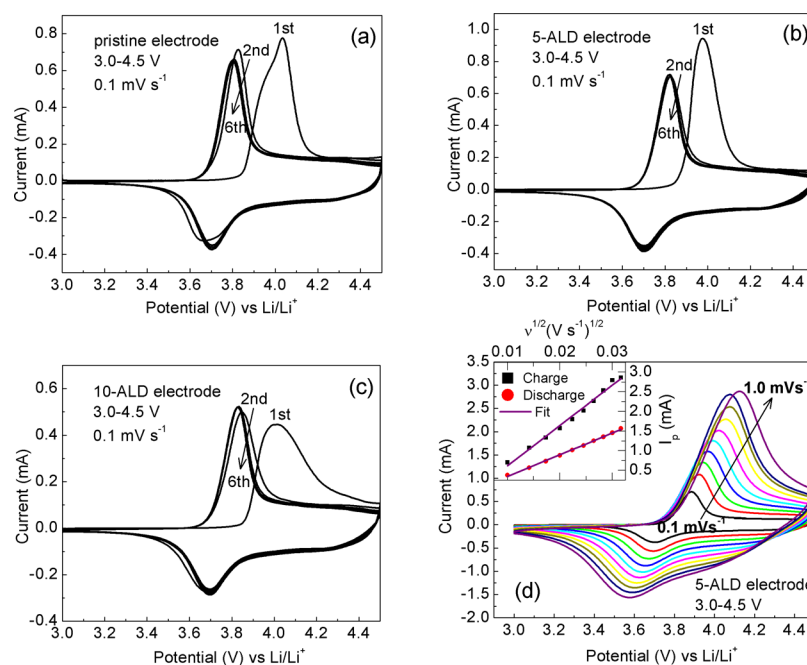
Figure 2. Cyclic voltammograms of (a) pristine, (b) 5-ALD, and (c) 10-ALD electrodes. (d) CVs of the 5-ALD electrode at various scan rates (0.1, 0.2, 0.3, 0.4, 0.5, 0.6, 0.7, 0.8, 0.9, and 1.0 mV s^{-1}). Inset: Dependence of the peak currents as a function of the square root of the scan rates in the charge region for the 5-ALD electrode.

shown in Figure 1, in which the pristine electrode exhibits relatively smooth surface characteristics in Figure 1a, while the sample coated with ALD Al$_2$O$_3$ clearly shows a uniform coating layer with a thickness of about of 1−3 nm on the surface of NMC532 in Figure 1b. The alumina coating was amorphous without changing the material structure of NMC532, as proven by XRD measurement (see Figure S1). The fast Fourier transformation (FFT) and lattice fringes in the inset of Figure 1 correspond to 0.47 and 0.23 nm d spacings, which are ascribed to the (003) and (012) planes of NMC532, indicating that the ALD process has no effect on the cathode crystal structure.

The interfacial electrochemistry properties of NMC532 with and without ALD Al$_2$O$_3$ were investigated by CV and EIS. CV scans of the pristine, 5-ALD, and 10-ALD electrodes were measured between 3.0 and 4.5 V (versus Li/Li$^+$) with a sweep rate of 0.1 mV s^{-1} during the first to sixth cycles, as shown in Figure 2a−c. The CV curves obtained for the pristine and ALD-coated NMC532 electrodes show differences between the redox peaks. The anodic (oxidation) peak is a result of the lithium extraction process, while the cathodic (reduction) peak corresponds to the lithium insertion process. In the first scan, the redox peaks of the pristine electrode were centered at 4.033 and 3.657 V, giving a potential difference of 0.376 V. However, the potential difference between two peaks decreased to 0.128 V in the second cycle and further decreased to 0.093 V in the sixth cycle. The differences between the cathodic and anodic peaks became larger when the thickness of the ALD Al$_2$O$_3$ coating on NMC532 electrodes increased from 5 to 10 ALD cycles (see Table S1), which suggested that the increase of the degree of electrochemical polarization was due to the lower electrical conductivity of ALD Al$_2$O$_3$. For example, NMC532 materials coated with thinner ALD Al$_2$O$_3$ displayed a lower difference between the redox peaks, indicating lower electrochemical polarization. Thus, an optimized thickness of the Al$_2$O$_3$ coating was required to achieve a balance between the electrochemical polarization and the enhancement of the

interfacial stability to improve the cycling performance for the NMC cathode.

The lithium diffusion properties of NMC532 with and without ALD Al$_2$O$_3$ were investigated by CV and GITT methods (Figure S2). Using the method of the CV scan rates ($\nu^{1/2}$) versus the peak current (I_p), the lithium-ion diffusion properties of NMC532 with and without ALD Al$_2$O$_3$ can be compared according to eq 1:

$$I_p = 2.69 \times 10^5 \times n^{3/2} A D^{1/2} \nu^{1/2} \Delta C \tag{1}$$

where n is the number of electrons in the specific electrochemical reactions, A is the electrode area (cm^2), D is the diffusion coefficient of lithium, which needs to be calculated, and ΔC is the change in the lithium concentration in the related reactions. When this equation was applied to CV scan rates obtained for an ALD Al$_2$O$_3$-coated NMC532 electrode, clearly a linear relationship existed between the peak current and scan rate, indicating diffusion-controlled behavior, as shown in the inset of Figures 2d and S3. It was clear that the coating thickness had a pronounced effect on lithium diffusion into the cathode materials. Stepwise increasing the scan rate from 0.1 to 1.0 mV s^{-1} with a step size of 0.1 mV s^{-1}, a clear shift to the higher (lower) potential end for the oxidation (reduction) peak was observed. The observed shift could be attributed to the high electrochemical polarization at NMC532/ALD Al$_2$O$_3$ interfaces, which occurred as a result of the lagging lithium diffusion rate following faster CV scan rate. Using the slope of the linear fits previously acquired, lithium diffusion coefficients in the electrodes were calculated and are presented in Table 1. The obtained lithium diffusion values indicated that diffusions between the pristine and ALD Al$_2$O$_3$-coated NMC532 electrodes were similar: there was only a small decrease for the ALD coating by the CV scan method but a small increase by the GITT method (Figure S2), providing clear evidence that the ALD coating did not significantly hinder lithium diffusion during the extraction/

C

Table 1. Lithium Diffusion Coefficients (cm² s⁻¹) of the Pristine, 5-ALD, and 10-ALD Electrodes in the Charging and Discharging Regions

sample	charge	discharge
pristine electrode	2.48×10^{-10}	7.92×10^{-11}
5-ALD electrode	1.85×10^{-10}	5.33×10^{-11}
10-ALD electrode	1.40×10^{-10}	5.32×10^{-11}

insertion process. This proves to be a significant advantage in using an ultrathin conformal ALD Al_2O_3 coating.

The stability enhancement of NMC532 with the ALD Al_2O_3 coating was most visible from the electrochemical performance. The cycling performance of the pristine and ALD-coated electrodes was measured with a 0.5 C rate with a cycling potential range from 3.0 to 4.5 V versus Li/Li⁺, respectively (Figure 3). The capacity, Coulombic efficiency, and rate
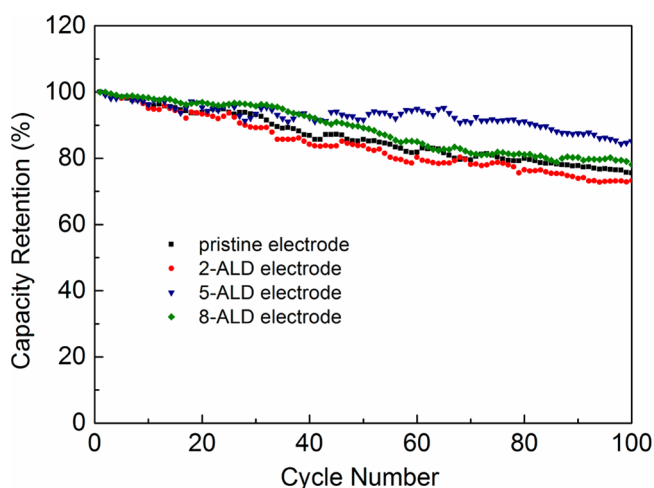
Figure 3. Capacity retained after 100 cycles at a 0.5 C rate between 3.0 and 4.5 V for different electrodes.

performance were also presented (see Figures S4 and S5). After 100 cycles, the capacity retention of the 5-ALD Al_2O_3 NMC532 electrode was about 85%, compared with only 75% for the pristine electrode. However, alumina coatings grown by wet-

chemical techniques with thicknesses of 4, 5, and even 20−30 nm (~20 times greater than the ALD maximum thickness) displayed noticeable stability improvement.[29−31] It was clear that the high purity and conformal nature of Al_2O_3 grown by ALD was able to protect material surfaces by using less material than conventional deposition techniques with less electrochemical polarization.

To further understand the factors that led to the improved electrochemical performance of these ALD-coated electrodes, EIS was also used to investigate their electrochemical resistance and lithium-ion diffusion kinetics at the electrode/electrolyte interfaces. In order to eliminate the influence of the formed thick SEI from a lithium metal anode, especially at the high-frequency regime,[32] we used the three-electrode cell (MTI Corp.) for the impedance measurement. The EIS measurements were conducted after the initial and 100th charging cycles to 4.5 V, and the results are shown in parts a and b of Figure 4, respectively. All of the Nyquist plots show two typical semicircles during the charge/discharge process. According to the previous EIS studies on these types of layered cathode materials,[33] the first semicircle was attributed to lithium-ion diffusion through the surface layer and electrons through the active material, and the second semicircle was assigned to the charge-transfer reaction. The EIS profile can be expressed by several parts from the high-to-low-frequency region. The corresponding equivalent circuit is given in Figure 4c, in which R_{sol} refers to the uncompensated ohmic resistance of the electrolyte, $R_{sf} \| CPE_{sf}$ represents the impedance for lithium-ion diffusion in the surface layer (including the SEI and surface modification layers), $R_{ct} \| CPE_{ct}$ refers to the charge-transfer resistance and charge-transfer capacitance, and Z_w represents the Warburg impedance describing the lithium-ion diffusion in the bulk material. Among these parameters, R_{sol}, R_{ct}, and Z_w can be used to quantify the ohmic polarization, charge-transfer polarization, and diffusion polarization, respectively.[34,35] The fitted impedance parameters are listed in Table 2. It is clear that there is a larger reduction in the charge-transfer resistance for the 5-ALD electrode than for the pristine electrode during upper charge cutoff voltages to 4.5 V. Note that the charge-transfer resistance for the 10-ALD electrode has a small increase due to the thicker Al_2O_3 coating. After 100 charging/
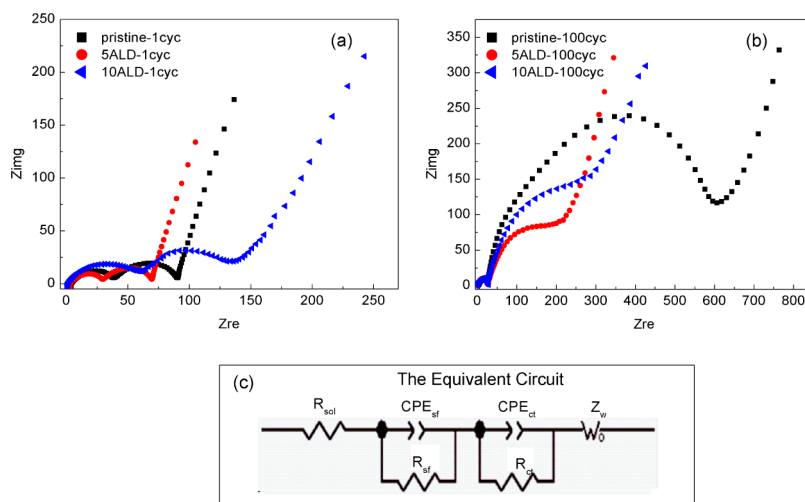

Figure 4. Nyquist plots for different electrodes: (a) after an initial charging to 4.5 V at a 0.1 C rate; (b) after charging to 4.5 V after 100 cycles at a 0.5 C rate. (c) Equivalent circuit performed to fit the curves.

Table 2. Impedance Parameters of the Pristine and ALD-Coated Electrodes after the Initial and 100th Charging Cycles to 4.5 V

sample	1 cycle			100 cycles		
	$R_{sol}(\Omega)$	$R_{sf}(\Omega)$	$R_{ct}(\Omega)$	$R_{sol}(\Omega)$	$R_{sf}(\Omega)$	$R_{ct}(\Omega)$
pristine electrode	4.10	36.75	48.75	3.68	23.04	564
5-ALD electrode	3.16	28.27	37.50	1.49	25.23	108
10-ALD electrode	1.19	55.23	80.09	1.76	26.01	243

discharging cycles, the charge-transfer resistance for the ALD Al_2O_3-coated NMC532 electrodes does not notably increase, while that of the pristine electrode shows a huge increase. This clearly reveals that the interfacial stability of NMC532 with the 5-ALD coating with consistent charge-transfer resistance was significantly enhanced compared with that of NMC532 without the ALD coating, leading to improvement of the electrochemical performance.

The mechanism of the stability difference at the interface between the electrolyte and NMC532 with and without the ALD Al_2O_3 coating was further investigated by XPS, which is another powerful technique for probing the chemical nature of the electrochemical interface in a LIB system. XPS of charged electrodes was carried out to determine the chemical composition of the NMC532 surface formed as a result of

high-voltage charging. A significant change was expected to occur upon high-voltage charging with surface species formation with oxidation of the electrolyte. Because of the limitation of the depth of penetration for XPS, the electrolyte oxidation products on the surface may screen some signals from the surface of the particles.[36] The Ni 2p, Mn 2p, and Co 2p spectra of XPS from the pristine as-received electrode and the electrode charged to 4.5 V are shown in parts a−c and d−f in the Figure 5, respectively. Note that while the pristine electrode was charged to 4.5 V, only the Ni 2p (Ni^{2+}) signal of the NiO composition was detected at the initial surface layer. After argon-ion sputtering to the deeper (about 30 nm from the surface) layer, the Co 2p and Mn 2p signals can be detected. All XPS signals of Ni 2p, Co 2p, and Mn 2p from the ALD Al_2O_3-coated electrode are shown in Figure 5g−i, which are the same as those of the original pristine electrode. Thus, the NMC532/electrolyte interfacial reaction can be retarded by ALD Al_2O_3. On the other hand, the surface characteristic even for oxygen species is one of the contributing factors that affect the electrochemical performance.[37] The lattice O 1s signal in the NMC532 pristine electrode by XPS was weakened after the initial charging, suggesting that electrolyte oxidation at the NMC532 interface occurs during the initial charging (see Figure S6). This is consistent with the resistance increase, as observed by EIS measurements (shown in Table 2). By
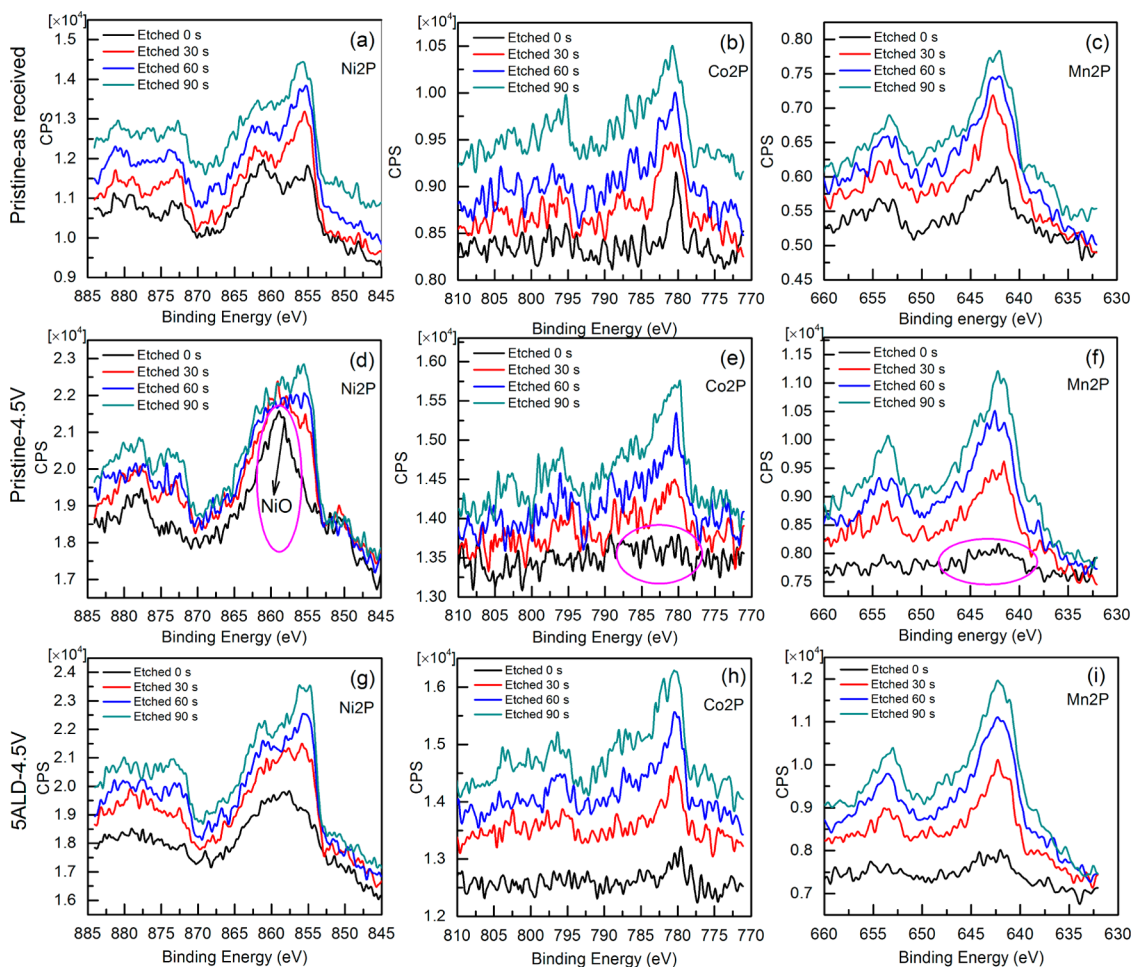

Figure 5. XPS Ni 2p, Co 2p, and Mn 2p peaks from NMC532-based electrodes: (a−c) pristine electrode as received; (d−f) pristine electrode after charging to 4.5 V; (g−i) 5-ALD electrode after charging to 4.5 V. Black line: prior to argon-ion sputtering. Red line: after 30 s argon-ion sputtering. Blue line: after 60 s argon-ion sputtering. Dark-cyan line: after 90 s argon-ion sputtering.
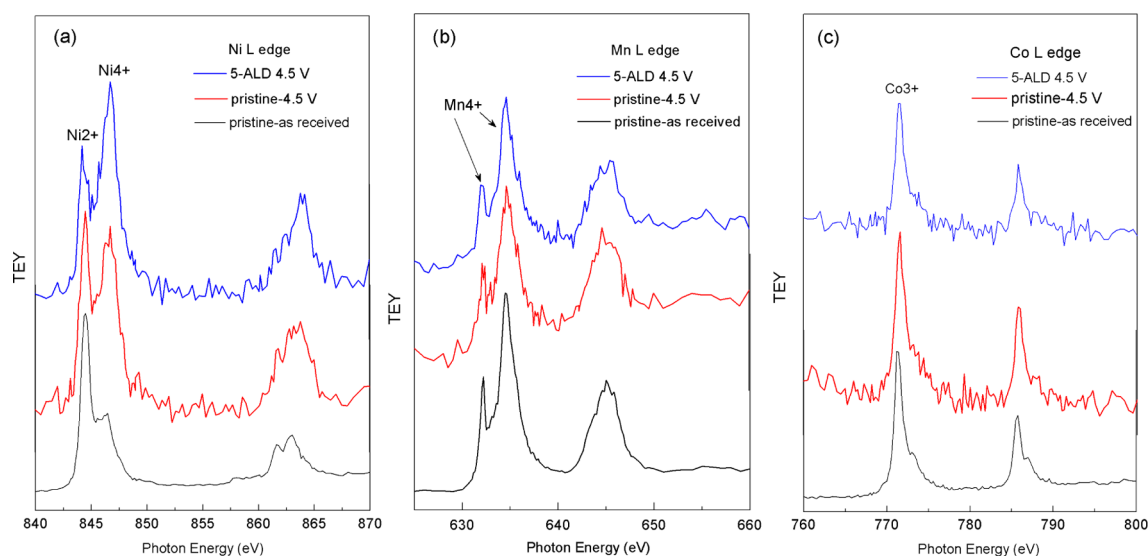
Figure 6. XAS Ni L-edge (a), Mn L-edge (b), and Co L-edge (c) from NMC532-based electrodes.
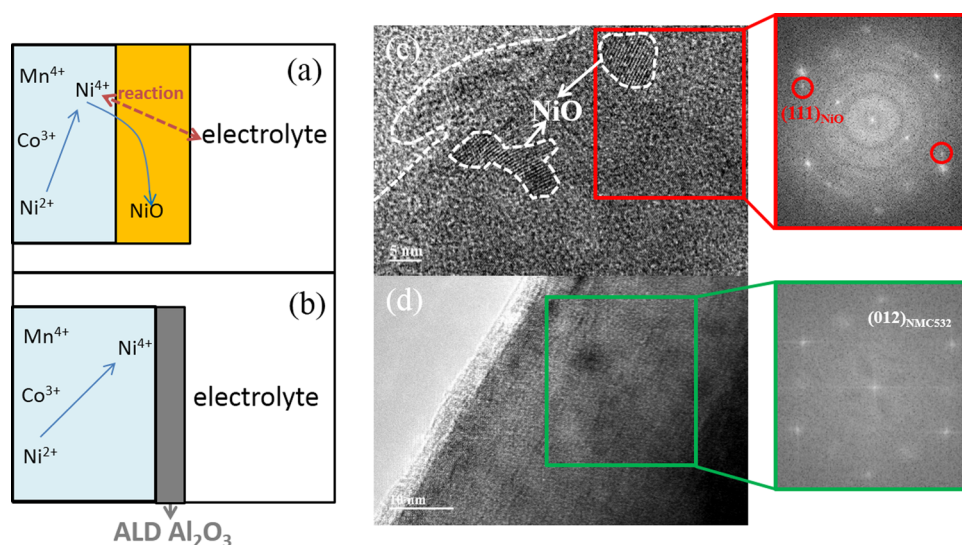

Figure 7. Schematic of (a) pristine and (b) ALD Al_2O_3-coated NMC532 electrodes after charging to high-voltage conditions. HRTEM images and FFTs after 100 cycles under 3.0−4.5 V conditions of the surface for (c) pristine and (d) ALD Al_2O_3-coated NMC532 electrodes.

contrast, the lattice O 1s signals for ALD Al_2O_3-coated NMC532 electrodes have no detectable change. The Al 2p peak after the cycle in XPS is shown in Figure S5. The Al 2p peak of the 5-ALD Al_2O_3-coated electrode shows a distinct reduction in the intensity upon cycling, which is consistent with the results in the literature.[38,39] The ALD Al_2O_3 layer bridged to the NMC532 substrate via an oxygen bond.[40] The Al $2p_{3/2}$ core-level XPS spectrum shows a binding energy of 75.1 eV for the Al_2O_3-coated electrode (Figure S7). Taking the O 1s peak (532.2 eV) into consideration (Figure S6), the chemical composition of the surface coating was confirmed to be Al_2O_3. After 100 cycles (between 3.0 and 4.5 V), the binding energy of the Al $2p_{3/2}$ core level did not show a noticeable shift, indicating a stable Al_2O_3 surface film against the electrochemical charge and discharge. The less electrolyte oxidation occurs, the lower the resistance and the better the electrochemical performance. This again indicates that the existence of Al_2O_3 coatings on the electrode surface can prevent electrolyte oxidation at the NMC532 interface.

XAS is another powerful technique for probing the chemical nature of the electrochemical interface in a LIB system. All of the spectra were collected in both surface-sensitive TEY and bulk-sensitive TFY modes. The probing depth about TEY was around 10 nm, and that about TFY was around 150 nm. All of the spectra were normalized to the photon flux measured by the photocurrent of an upstream gold mesh. The TEY- and TFY-mode Ni L-edge spectra of XAS from the pristine electrode as-received and charged to 4.5 V are shown in Figures 6a and S8, respectively. When the pristine electrode was charged to 4.5 V, the Ni^{2+} signal was stronger than the Ni^{4+} signal at the initial surface layer, indicated that electrolyte oxidation at the NMC532 interface occurs during the initial charging. This is consistent with the XPS measurements. However, for NMC532 coated with ALD Al_2O_3, the Ni^{4+} signals were much stronger than the Ni^{2+} signals, suggesting that the NMC532/electrolyte interfacial reaction can be retarded by ALD Al_2O_3. Besides, the TEY mode Mn and Co L-edge spectra of XAS from the as-received electrode and the electrode charged to 4.5 V are shown in Figure 6b,c. The valences of Mn and Co for the

pristine electrode are 3+ and 4+, respectively. After charging to a high voltage of 4.5 V, the valences of Co and Mn are not changed with and without the ALD Al_2O_3 coating, indicating that degradation of NMC532 was mainly related with the Ni element.[40] On the basis of these results, it is concluded that Al_2O_3 surface coatings on the electrodes by the ALD process play an important role in improving the electrochemical performance because of suppression of the electrolyte oxidation to decrease the resistance, especially for the charge-transfer resistance.

The mechanism of interfacial interaction between the electrolyte and NMC532 with and without the ALD Al_2O_3 coating during charging to high voltage (around 4.5 V) is schematically illustrated in Figure 7. In the case of the pristine NMC532 electrode, the valence of Ni in NMC532 was raised initially from Ni^{2+} and Ni^{3+} to Ni^{4+} during charging to a high voltage of about 4.5 V, and then the Ni^{4+} ions around the NMC532 surface can accelerate the interfacial reaction with the electrolyte because of the Ni^{4+} higher oxidation features, in order to be reduced to form the rock-salt phase, a NiO new microstructure phase at the surface of the electrode, as shown in Figure 7a. The new microphase generated around the NMC532 surface was observed by TEM (Figure 7c). The interfacial reaction with the electrolyte to form the rock-salt phase (NiO) can also be found in ref 41. The presence of the ionically blocking rock-salt phase inhibits the motion of lithium ions to increase the interfacial resistance. With the ALD Al_2O_3-coated electrodes, while interfacial reactions with the electrode are prevented, formation of the rock-salt phase was not observed by TEM, as shown in Figure 7b,d. Besides retarding the interfacial reaction, the ALD Al_2O_3 coatings can also inhibit (may not entirely prevent) the dissolution of transition-metal ions and HF attack. However, the degradation mechanism of NMC532 is different from that of the other cathode materials, even for the other NMCs. The main cause of NMC532 degradation at high voltage was not related with transition-metal dissolution.[41] The phase transformation was the key process under high voltage. As a consequence, the protective layer of the Al_2O_3 film on the electrode surface could enhance the electrode surface stability to improve the cycling performance.

4. CONCLUSIONS

In summary, the ALD Al_2O_3-coated NMC532 electrode shows better capacity retention than the pristine electrode during charging/discharging around the potential range of 3.0−4.5 V (high voltage). By using XPS, XAS, and electrochemical methods, we investigated the surface structures with and without an ALD Al_2O_3-coated NMC532 electrode after charging/discharging and related electrochemistry properties and found that the ultrathin ALD Al_2O_3 film could reduce the interfacial resistance of lithium-ion diffusion and enhance the surface stability of NMC532 by retarding reactions of NMC532/electrolyte interfaces to prevent the formation of new microstructure rock-salt phase NiO around the NMC532 surfaces.

ASSOCIATED CONTENT

Ⓢ Supporting Information

The Supporting Information is available free of charge on the ACS Publications website at DOI: 10.1021/acsami.5b05500.

Potentials of the redox peaks, XRD patterns, lithium-ion diffusion coefficient (D_{Li}^+) measured by GITT, CV curves, discharge capacity and Coulombic efficiency, rate capacity, O 1s XPS spectra, Al 2p XPS spectra for a 5-ALD electrode, and XAS Ni L-edge from NMC532-based electrodes (PDF)

AUTHOR INFORMATION

Corresponding Authors

*E-mail: wangxw@pkusz.edu.cn (X.W.).
*E-mail: panfeng@pkusz.edu.cn (F.P.).

Notes

The authors declare no competing financial interest.

REFERENCES

(1) Ohzuku, T.; Makimura, Y. Layered Lithium Insertion Material of $LiNi_{1/2}Mn_{1/2}O_2$: A Possible Alternative to $LiCoO_2$ for Advanced Lithium-Ion Batteries. *Chem. Lett.* **2001**, 8, 744−745.

(2) Lu, Z. H.; MacNeil, D. D.; Dahn, J. R. Layered Li-$[Ni_xCo_{1-2x}Mn_x]O_2$ Cathode Materials for Lithium-Ion Batteries. *Electrochem. Solid-State Lett.* **2001**, 4, A200−A203.

(3) Wang, L.; Li, J.; He, X.; Pu, W.; Wan, C.; Jiang, C. Recent Advances in Layered $LiNi_xCo_yMn_{1-x-y}O_2$ Cathode Materials for Lithium Ion Batteries. *J. Solid State Electrochem.* **2009**, 13, 1157−1164.

(4) Wu, Z. Z.; Ji, S. P.; Zheng, J. X.; Hu, Z. X.; Xiao, S.; Wei, Y.; Zhuo, Z. Q.; Lin, Y.; Yang, W. L.; Xu, K.; Amine, K.; Pan, F. Prelithiation Activates $Li(Ni_{0.5}Mn_{0.3}Co_{0.2})O_2$ for High Capacity and Excellent Cycling Stability. *Nano Lett.* **2015**, 15, 5590−5596.

(5) Zhou, F.; Zhao, X.; Smith, A. J.; Dahn, J. R. Studies of $LiNi_{2/3}Mn_{1/3}O_2$: A Positive Electrode Material that Cycles Well to 4.6 V. *J. Electrochem. Soc.* **2010**, 157, A399−A406.

(6) Wei, Y.; Zheng, J. X.; Cui, S. H.; Song, X. H.; Su, Y. T.; Deng, W. J.; Wu, Z. Z.; Wang, X. W.; Wang, W. D.; Rao, M. M.; Lin, Y.; Wang, C. M.; Amine, K.; Pan, F. Kinetics Tuning of Li-ion Diffusion in Layered $Li(Ni_xMn_yCo_z)O_2$. *J. Am. Chem. Soc.* **2015**, 137, 8364−8367.

(7) Sun, Y.-K.; Cho, S.-W.; Lee, S.-W.; Yoon, C. S.; Amine, K. AlF_3-Coating to Improve High Voltage Cycling Performance of Li-$[Ni_{1/3}Co_{1/3}Mn_{1/3}]O_2$ Cathode Materials for Lithium Secondary Batteries. *J. Electrochem. Soc.* **2007**, 154, A168−A172.

(8) Li, X.; Liu, J.; Meng, X.; Tang, Y.; Banis, M. N.; Yang, J.; Hu, Y.; Li, R.; Cai, M.; Sun, X. Significant Impact on Cathode Performance of Lithium-Ion Batteries by Precisely Controlled Metal Oxide Nanocoatings via Atomic Layer Deposition. *J. Power Sources* **2014**, 247, 57−69.

(9) Kawamura, T.; Okada, S.; Yamaki, J.-I. Decomposition Reaction of $LiPF_6$-based Electrolytes for Lithium Ion Cells. *J. Power Sources* **2006**, 156, 547−554.

(10) Xu, W.; Vegunta, S. S. S.; Flake, J. C. Surface-Modified Silicon Nanowire Anodes for Lithium-Ion Batteries. *J. Power Sources* **2011**, 196, 8583−8589.

(11) Lux, S. F.; Lucas, I. T.; Pollak, E.; Passerini, S.; Winter, M.; Kostecki, R. The Mechanism of HF Formation in $LiPF_6$ Based Organic Carbonate Electrolytes. *Electrochem. Commun.* **2012**, 14, 47−50.

(12) Lee, B. R.; Noh, H. J.; Myung, S. T.; Amine, K.; Sun, Y. K. High-Voltage Performance of $Li[Ni_{0.55}Co_{0.15}Mn_{0.30}]O_2$ Positive Electrode

Material for Rechargeable Li-Ion Batteries. *J. Electrochem. Soc.* **2011**, *158*, A180−A186.

(13) Zheng, J. X.; Hou, Y. Y.; Duan, Y. D.; Song, X. H.; Wei, Y.; Liu, T. C.; Hu, J. T.; Guo, H.; Zhuo, Z. Q.; Liu, L. L.; Chang, Z.; Wang, X. W.; Zherebetskyy, D.; Fang, Y. Y.; Lin, Y.; Xu, K.; Wang, L.-W.; Wu, Y. P.; Pan, F. Janus Solid−Liquid Interface Enabling Ultrahigh Charging and Discharging Rate for Advanced Lithium-Ion Batteries. *Nano Lett.* **2015**, *15*, 6102−6109.

(14) Hirayama, M.; Sakamoto, K.; Hiraide, T.; Mori, D.; Yamada, A.; Kanno, R.; Sonoyama, N.; Tamura, K.; Mizuki, J. Characterization of Electrode/Electrolyte Interface Using in situ X-Ray Reflectometry and $LiNi_{0.8}Co_{0.2}O_2$ Epitaxial Film Electrode Synthesized by Pulsed Laser Deposition Method. *Electrochim. Acta* **2007**, *53*, 871−881.

(15) Shaju, K. M.; SubbaRao, G. V.; Chowdari, B. V. R. Performance of Layered $Li(Ni_{1/3}Co_{1/3}Mn_{1/3})O_2$ as Cathode for Li-Ion Batteries. *Electrochim. Acta* **2002**, *48*, 145−151.

(16) Wang, H.; Jang, Y. I.; Huang, B.; Sadoway, D. R.; Chiang, Y. M. TEM Study of Electrochemical Cycling-Induced Damage and Disorder in $LiCoO_2$ Cathodes for Rechargeable Lithium Batteries. *J. Electrochem. Soc.* **1999**, *146*, 473−480.

(17) Li, J.; Fan, M.; He, X.; Zhao, R.; Jiange, C.; Wan, C. TiO_2 Coating $LiNi_{1/3}Co_{1/3}Mn_{1/3}O_2$ Cathode Materials for Li-Ion Batteries. *Ionics* **2006**, *12*, 215−218.

(18) Riley, L. A.; Van Atta, S.; Cavanagh, A. S.; Yan, Y.; George, S. M.; Liu, P.; Dillon, A. C.; Lee, S.-H. Electrochemical Effects of ALD Surface Modification on Combustion Synthesized $LiNi_{1/3}Mn_{1/3}Co_{1/3}O_2$ as a Layered-Cathode Material. *J. Power Sources* **2011**, *196*, 3317−3324.

(19) Wu, Y.; Wen, Z.; Li, J. Hierarchical Carbon-Coated $LiFePO_4$ Nanoplate Microspheres with High Electrochemical Performance for Li-Ion Batteries. *Adv. Mater.* **2011**, *23*, 1126−1129.

(20) Scott, I. D.; Jung, Y. S.; Cavanagh, A. S.; Yan, Y.; Dillon, A. C.; George, S. M.; Lee, S.-H. Ultrathin Coatings on Nano-$LiCoO_2$ for Li-Ion Vehicular Applications. *Nano Lett.* **2011**, *11*, 414−418.

(21) Jung, Y. S.; Lu, P.; Cavanagh, A. S.; Ban, C.; Kim, G.-H.; Lee, S.-H.; George, S. M.; Harris, S. J.; Dillon, A. C. Unexpected Improved Performance of ALD Coated $LiCoO_2$/Graphite Li-Ion Batteries. *Adv. Energy Mater.* **2013**, *3*, 213−219.

(22) Bettge, M.; Li, Y.; Sankaran, B.; Rago, N. D.; Spila, T.; Haasch, R. T.; Petrov, I.; Abraham, D. P. Improving High-Capacity $Li_{1.2}Ni_{0.15}Mn_{0.55}Co_{0.1}O_2$-Based Lithium-Ion Cells by Modifying the Positive Electrode with Alumina. *J. Power Sources* **2013**, *233*, 346−357.

(23) Jung, Y. S.; Cavanagh, A. S.; Riley, L. A.; Kang, S.-H.; Dillon, A. C.; Groner, M. D.; George, S. M.; Lee, S.-H. Ultrathin Direct Atomic Layer Deposition on Composite Electrodes for Highly Durable and Safe Li-Ion Batteries. *Adv. Mater.* **2010**, *22*, 2172−2176.

(24) Meng, X.; Yang, X. Q.; Sun, X. Emerging Applications of Atomic Layer Deposition for Lithium-Ion Battery Studies. *Adv. Mater.* **2012**, *24*, 3589−3615.

(25) Chen, Z.; Qin, Y.; Amine, K.; Sun, Y. K. Role of Surface Coating on Cathode Materials for Lithium-Ion Batteries. *J. Mater. Chem.* **2010**, *20*, 7606−7612.

(26) Xiao, X. C.; Lu, P.; Ahn, D. Ultrathin Multifunctional Oxide Coatings for Lithium Ion Batteries. *Adv. Mater.* **2011**, *23*, 3911−3915.

(27) He, Y.; Yu, X. Q.; Wang, Y. H.; Li, H.; Huang, X. J. Alumina-Coated Patterned Amorphous Silicon as the Anode for a Lithium-Ion Battery with High Columbic Efficiency. *Adv. Mater.* **2011**, *23*, 4938−4941.

(28) Jung, Y. S.; Cavanagh, A. S.; Gedvilas, L.; Widjonarko, N. E.; Scott, I. D.; Lee, S.-H.; Kim, G.-H.; George, S. M.; Dillon, A. C. Improved Functionality of Lithium-Ion Batteries Enabled by Atomic Layer Deposition on the Porous Microstructure of Polymer Separators and Coating Electrodes. *Adv. Energy Mater.* **2012**, *2*, 1022−1027.

(29) Cho, J.; Kim, Y. J.; Park, B. Novel $LiCoO_2$ Cathode Material with Al_2O_3 Coating for a Li Ion Cell. *Chem. Mater.* **2000**, *12*, 3788−3791.

(30) Myung, S. T.; Izumi, K.; Komaba, S.; Sun, Y. K.; Yashiro, H.; Kumagai, N. Role of Alumina Coating on Li-Ni-Co-Mn-O Particles as Positive Electrode Material for Lithium-Ion Batteries. *Chem. Mater.* **2005**, *17*, 3695−3704.

(31) Wang, Z. X.; Liu, L. J.; Chen, L. Q.; Huang, X. J. Structural and Electrochemical Characterizations of Surface-Modified $LiCoO_2$ Cathode Materials for Li-Ion Batteries. *Solid State Ionics* **2002**, *148*, 335−342.

(32) Schmidt, J. P.; Chrobak, T.; Ender, M.; Illig, J.; Klotz, D.; Ivers-Tiffee, E. Studies on $LiFePO_4$ as Cathode Material Using Impedance Spectroscopy. *J. Power Sources* **2011**, *196*, 5342−5348.

(33) Zheng, J. M.; Zhang, Z. R.; Wu, X. B.; Dong, Z. X.; Zhu, Z.; Yang, Y. The Effects of AlF_3 Coating on the Performance of $Li[Li_{0.2}Mn_{0.54}Ni_{0.13}Co_{0.13}]O_2$ Positive Electrode Material for Lithium-Ion Battery. *J. Electrochem. Soc.* **2008**, *155*, A775−A782.

(34) Wang, Q. Y.; Liu, J.; Murugan, A. V.; Manthiram, A. High Capacity Double-Layer Surface Modified $Li[Li_{0.2}Ni_{0.13}Co_{0.13}Mn_{0.54}]O_2$ Cathode with Improved Rate Capability. *J. Mater. Chem.* **2009**, *19*, 4965−4972.

(35) Guo, S. H.; Yu, H. J.; Liu, P.; Liu, X. Z.; Li, D.; Chen, M. W.; Ishida, M.; Zhou, H. S. Surface Coating of Lithium−Manganese-Rich Layered Oxides with Delaminated MnO_2 Nanosheets as Cathode Materials for Li-Ion Batteries. *J. Mater. Chem. A* **2014**, *2*, 4422−4428.

(36) Martha, S. K.; Nanda, J.; Veith, G. M.; Dudney, N. J. Surface Studies of High Voltage Lithium Rich Composition: $Li_{1.2}Mn_{0.525}Ni_{0.175}Co_{0.1}O_2$. *J. Power Sources* **2012**, *216*, 179−186.

(37) Fell, C. R.; Carroll, K. J.; Chi, M. F.; Meng, Y. S. Synthesis−Structure−Property Relations in Layered "Li-excess" Oxides Electrode Materials $Li[Li_{1/3−2x/3}Ni_xMn_{2/3−x/3}]O_2$ (x = 1/,1/4, and 1/5). *J. Electrochem. Soc.* **2010**, *157*, A1202−A1211.

(38) Bettge, M.; Li, Y.; Sankaran, B.; Rago, N. D.; Spila, T.; Haasch, R. T.; Petrov, I.; Abraham, D. P. Improving High-Capacity $Li_{1.2}Ni_{0.15}Mn_{0.55}Co_{0.1}O_2$-based Lithium-Ion Cells by Modifiying the Positive Electrode with Alumina. *J. Power Sources* **2013**, *233*, 346−357.

(39) Zhang, X. F.; Belharouak, I.; Li, L.; Lei, Y.; Elam, J. W.; Nie, A.; Chen, X. Q.; Yassar, R. S.; Axelbaum, R. L. Structural and Electrochemical Study of Al_2O_3 and TiO_2 Coated $Li_{1.2}Ni_{0.13}Mn_{0.54}Co_{0.13}O_2$ Cathode Material Using ALD. *Adv. Energy. Mater.* **2013**, *3*, 1299−1307.

(40) Wu, Z. Z.; Han, X. G.; Zheng, J. X.; Wei, Y.; Qiao, R. M.; Shen, F.; Dai, J. Q.; Hu, L. B.; Xu, K.; Lin, Y.; Yang, W. L.; Pan, F. Depolarized and Fully Active Cathode Based on $Li(Ni_{0.5}Co_{0.2}Mn_{0.3})O_2$ Embedded in Carbon Nanotube Network for Advanced Batteries. *Nano Lett.* **2014**, *14*, 4700−4706.

(41) Jung, S. K.; Gwon, H.; Hong, J.; Park, K. Y.; Seo, D. H.; Kim, H.; Hyun, J.; Yang, W.; Kang, K. Understanding the Degradation Mechanisms of $LiNi_{0.5}Co_{0.2}Mn_{0.3}O_2$ Cathode Material in Lithium ion Batteries. *Adv. Energy. Mater.* **2014**, *4*, 1300787.